Analysis of test beam data using a technological prototype of a highly granular calorimeter and study of light quark production at a future linear collider

PhD Defense

Yuichi OKUGAWA

07/02/2024

Université Paris-Saclay & Tohoku University

My PhD work summary

Hardware work

- Assembling of 15 layer Silicon-Tungsten ECAL prototype.
- Commissioning of the prototype with over 15,000 silicon pixels.
- Analysis of beam test and simulation data.

Physics Analysis

- Analysis of $e^+e^- \to q\bar{q}$ simulation for the International Linear Collider.
- Exploration of analysis technique first time for the light quark pair production process.

Table of contents

Introduction

The Standard Model of Particle Physics

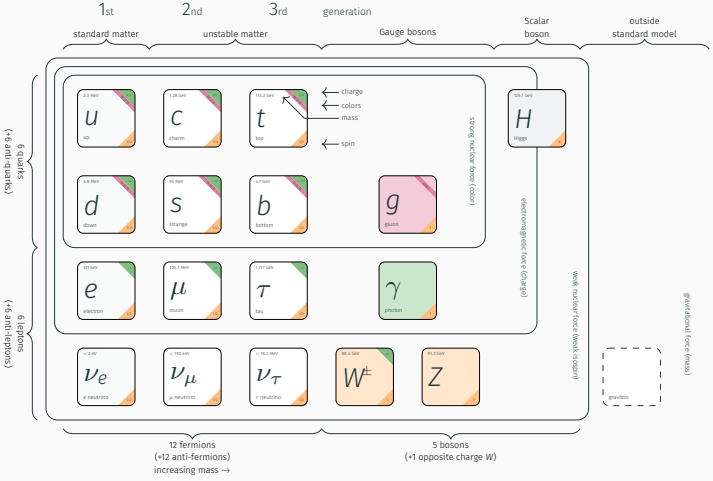

The Standard Model of Particle Physics

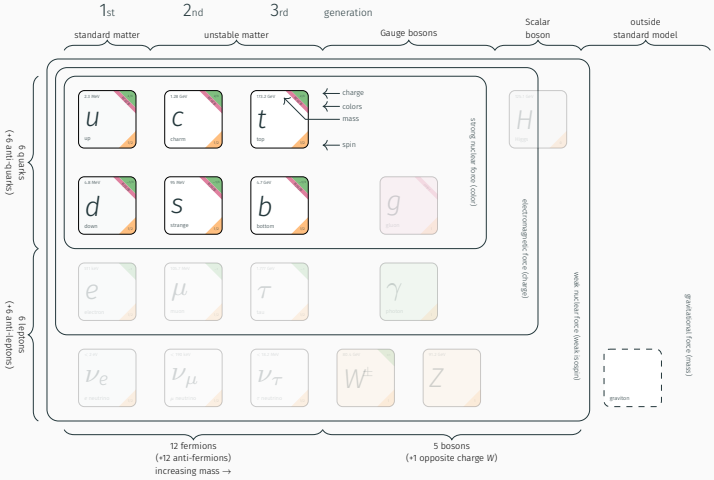

The Standard Model of Particle Physics

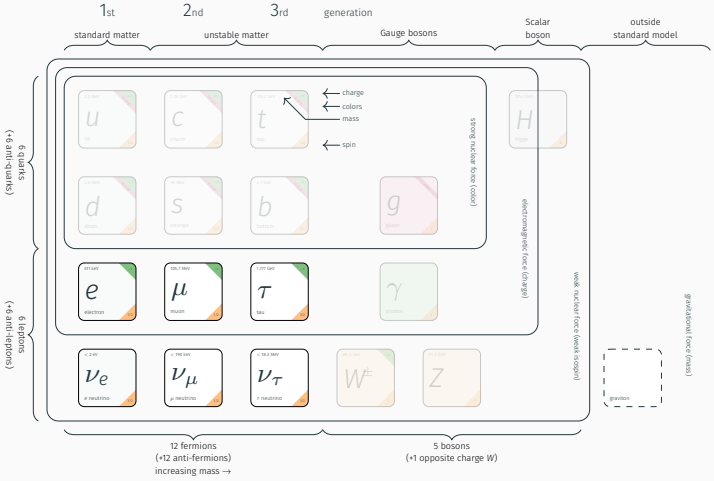

The Standard Model of Particle Physics

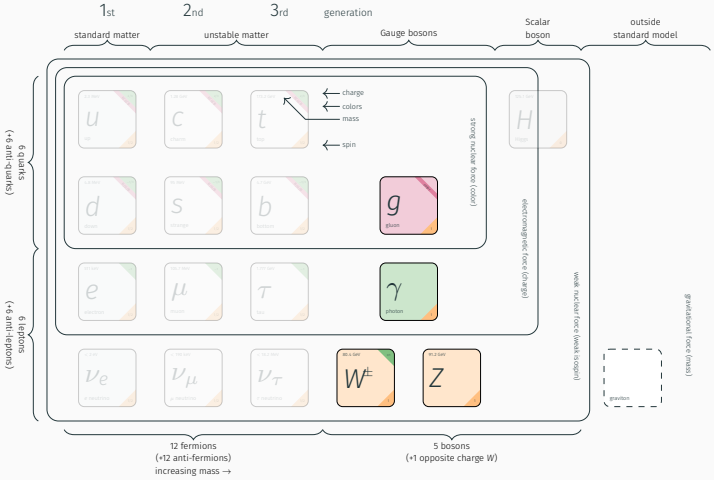

The Standard Model of Particle Physics

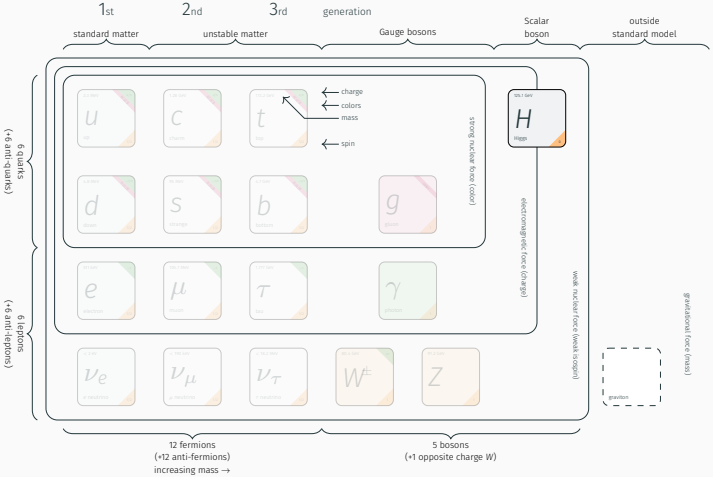

Gauge Theory

Standard Model is founded upon on the **gauge symmetry**:

$$SU(3)_C \times SU(2)_L \times U(1)_Y$$

- $\mathrm{SU(3)_C}$ gauge group describes the strong interactions.
- $\mathrm{SU(2)_L \times U(1)_Y}$ describes the electroweak interaction.

Gauge invariance requires gauge bosons to be massless.

→ They're not! Z and W bosons are massive.

Explanation of gauge boson masses are contained within the Higgs mechanism.

→ Higgs boson was discovered by the LHC experiments in 2012 at 125 GeV.

Open Questions to the Universe

Open questions to the universe

- ☑ Where is Higgs boson? $\rightarrow$ Yes!
- ☑ Do neutrinos have mass? $\rightarrow$ Yes!
- ☐ Where/what are the dark matters?
- ☐ How come gravity so weak?
- ☐ Why matter dominates the universe?
- ☐ Why is Higgs boson so light?
- ☐ Fermion mass hierarchy problem.

BSM and Fermion Mass Hierarchy

- SM does not have answer to the mass hierarchy in the fermion sector.
- Various models with extra-dimensions need be probed with fundamental scale beyond 10 TeV.
- BSM theories predict Z' resonance coupling to heavy quark (t,b,c) and also to light quarks (s,d,u).
  - e.g. Randal Sundrum, Gauge Higgs Unification (GHU)

→ Precision measurement!

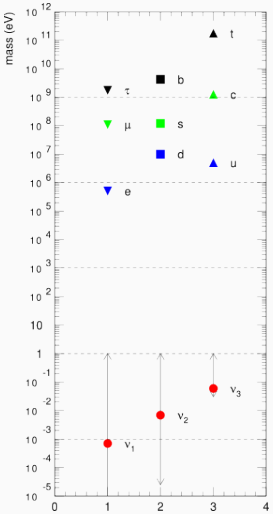

The ILC and ILD

Hadron Collider

- Composite particle collision
- Less control over the initial state
- Electroweak + strong interactions

Lepton Collider

- Elementary particle collision
- Full control over the initial state
- Electroweak interactions

ILC Description

- Future e^+e^- linear collider project.
- Enables polarization of both electron and positron beams.
- Push and pull configuration (ILD/SiD)
- Extendable linear facility to reach higher energies.

Precision Measurements

- Less QCD backgrounds compared to hadron colliders.
- Ability to polarize the beams can enhance cross section and reduce backgrounds.

Schematic view of ILC

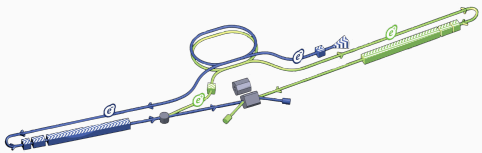

Parameter	Configuration
Site length	L_{site} =20.5–40 km
Center of mass energy	$\sqrt{s}$ =91.2–1000 GeV
Polarization	$(e^-, e^+) = (\pm 80\,\%, \mp 30\,\%)$
Luminosity	$\mathcal{L}$ =1.35–5.40 × 10^{34} cm^{-2} s^{-1}

Tracking System

- Vertex Detector (VTX)
- Central Silicon (SIT/SET)
- Time Projection Chamber (TPC)

Calorimeter System

- Electromagnetic Calorimeter (ECAL)
- Hadronic Calorimeter (HCAL)

Outer Instruments

- Muon Yoke
- Superconductive Coil

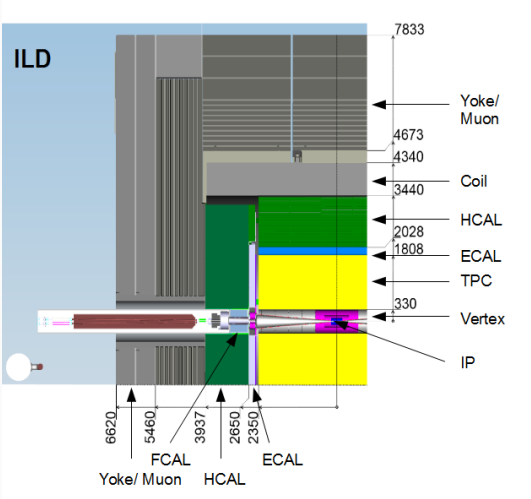

Tracking System

- Vertex Detector (VTX)
- Central Silicon (SIT/SET)
- Time Projection Chamber (TPC)

Calorimeter System

- Electromagnetic Calorimeter (ECAL)
- Hadronic Calorimeter (HCAL)

Outer Instruments

- Muon Yoke
- Superconductive Coil

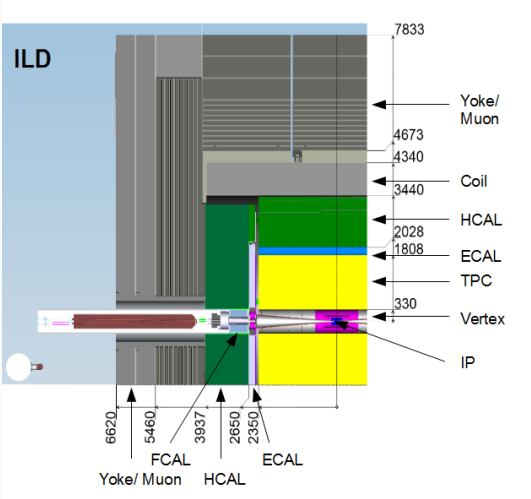

Tracking System

- Vertex Detector (VTX)
- Central Silicon (SIT/SET)
- Time Projection Chamber (TPC)

Calorimeter System

- Electromagnetic Calorimeter (ECAL)
- Hadronic Calorimeter (HCAL)

Outer Instruments

- Muon Yoke
- Superconductive Coil

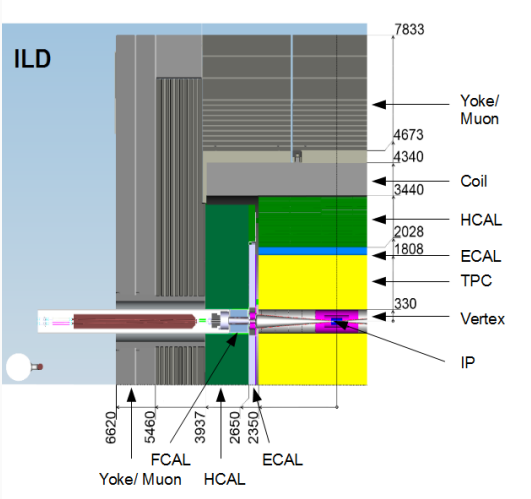

Tracking System

- Vertex Detector (VTX)
- Central Silicon (SIT/SET)
- Time Projection Chamber (TPC)

Calorimeter System

- Electromagnetic Calorimeter (ECAL)
- Hadronic Calorimeter (HCAL)

Outer Instruments

- Muon Yoke
- Superconductive Coil

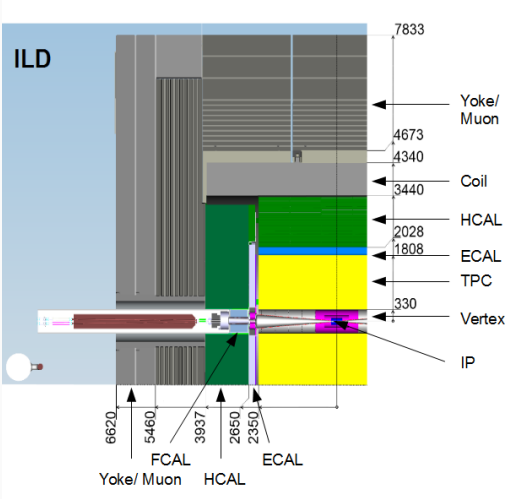

Jet energy composition

- Charged hadron: **60 %**
- Photon: **30 %**
- Neutral hadron: **10 %**

Pure calorimetric approach

- Measure all jet energy from ECAL and HCAL.
- ∼70 % of jet energy measured in HCAL.
- Jet energy resolution is heavily limited by calorimeter energy resolution.

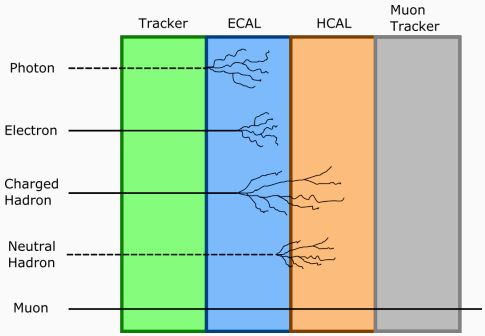

Particle Flow

- Measure energy of charged particles in tracker
- Photons in ECAL
- Neutral hadron in HCAL

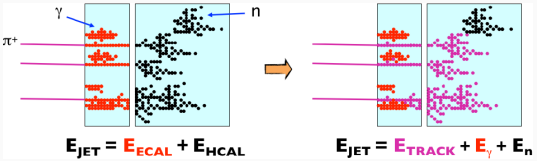

Requirements

- Jet energy resolution $\sigma_{E_{jet}}/E_{jet} \sim 3$–$4\,\%$ is demanded by physics requirements (i.e. Z/W mass separation).
- High granularity of calorimeters are absolutely necessary!

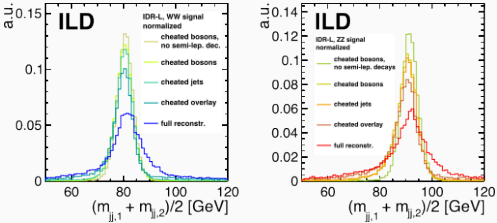

Silicon-Tungsten ECAL

Technical implementation

- **Tungsten (W)** as an absorber material
  - X_0 =3.5 mm
    - → A small radiation length to make ECAL as compact as $24X_0$ within 20 cm.
  - R_M =9 mm
    - → A small Molière radius to better separate nearby showers.
  - λ_I =96 mm → $\lambda_I/X_0 = 27.5$
    - → Clearly distinguish electromagnetic showers from hadronic ones.
- **Silicon (Si)** as an active material
  - Pixels with high granularity.
  - Robust technology.
  - Supports excellent signal/noise ratio.

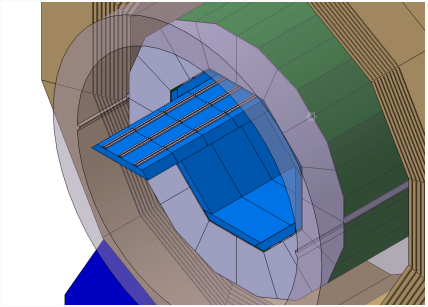

All future e^+e^- collider projects feature at least one detector concept with this technology.

Technical implementation

- **Tungsten (W)** as an absorber material
  - X_0 =3.5 mm
    - → A small radiation length to make ECAL as compact as $24X_0$ within 20 cm.
  - R_M =9 mm
    - → A small Molière radius to better separate nearby showers.
  - λ_I =96 mm → $\lambda_I/X_0 = 27.5$
    - → Clearly distinguish electromagnetic showers from hadronic ones.
- **Silicon (Si)** as an active material
  - Pixels with high granularity.
  - Robust technology.
  - Supports excellent signal/noise ratio.

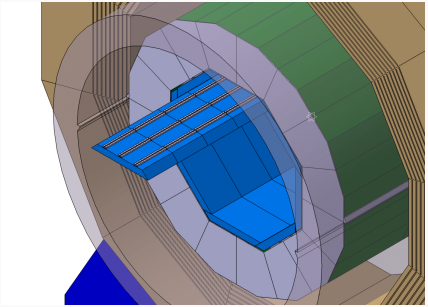

All future e^+e^- collider projects feature at least one detector concept with this technology.

ILD ECAL composition

- Sandwich structure
  (alternating active and absorber layer)
- Barrel + endcap modules
- Active Sensor Units (ASU)

- Calorimeter must be compact to fit inside the magnetic coil.
- Minimum active cooling but power pulsing.
  - Enabled by the ILC beam structure.

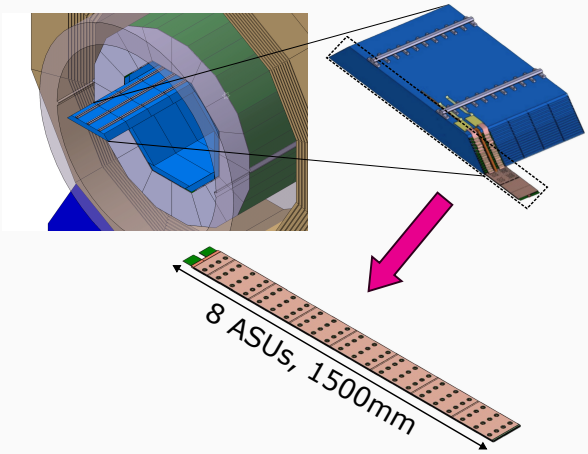

SiW-ECAL Structure

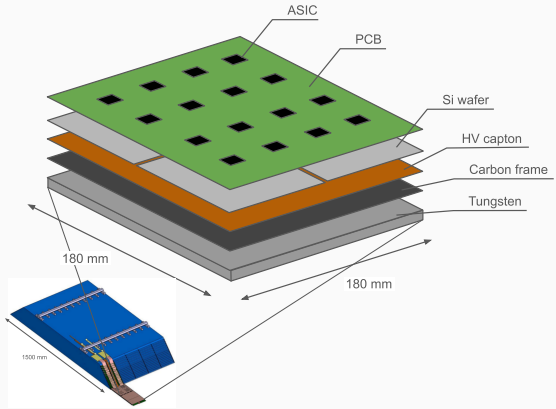

ASU structure

- PCB + ASICs + Si sensor + Copper/Kapton
- Composition:
  - 4 Si sensor plates / 1 ASU
  - 16 ASICs / 1 ASU
    $\rightarrow$ 4 ASICs readout from 1 sensor pad.
  - 64 pixels / 1 ASIC

Tungsten

- Supported by the frame, placed under the ASU.

Minimum Ionizing Particle (MIP)

- Mean energy loss rate in the matter is the minimum.
- Silicon with specific density 2.33 g cm^{-3}.
- 80 electron hole pairs per µm $\rightarrow$ 40 fC.

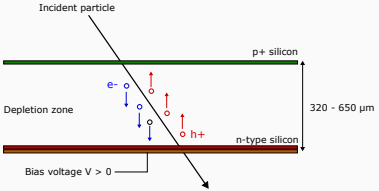

Silicon Sensor

- Silicon PIN diode sensors.
- Highly granular segmentation (5.5 × 5.5 mm^2).
- Glued to the PCB using the conductive adhesive.
- Bias voltage of 150 V.

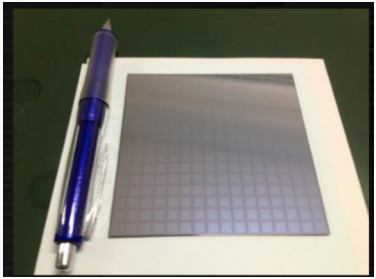

Application Specific Integrated Circuit (ASIC)

- Silicon Kalorimeter Integrated Read Out Chip (SKIROC).
- SiGe 0.35 µm AMS.
- Dimension 7.5 × 8.7 mm^2.
- Dual gain settings (high and low) covering large dynamic range of 0.5-3000 MIPs.
- Capable of auto-triggering at 1/2 MIP.
- Takes 15 event buffers for each cell.
- Consumes low power and compatible with “power pulsing” mode of ILC.

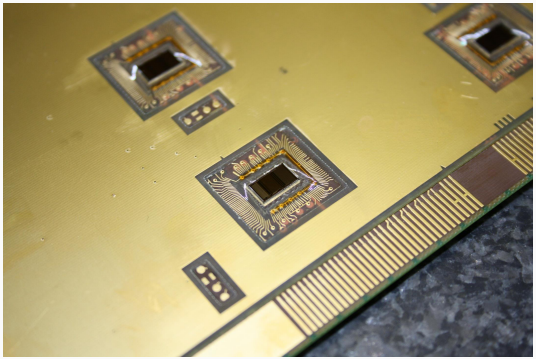

SiW-ECAL Prototype Structure

- Sensors
  - 15 layers
  - 16 chips / layer
  - 64 channel / chip
  - 15,360 total cells
- Tungsten: up to 20.4 X_0
- Digital readout boards developed in IJCLab, thanks to service electronique.

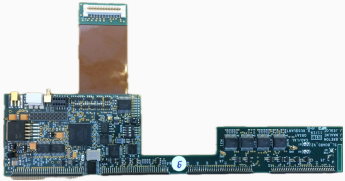

CALICE Collaboration

- **CA**lorimeter for a **LI**near **C**ollider **E**xperiment collaboration.
- Conducts R&D for highly granular electromagnetic and hadronic calorimeters.

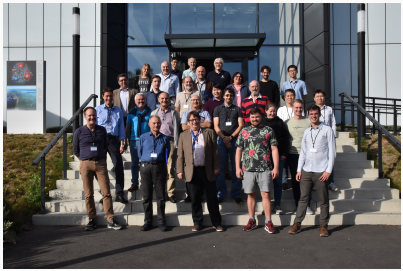

Prototype Developments

Physics Prototype

- Proof of principle.
- Developed from 2005 - 2011.
- 9 silicon sensors, subdivided into 6 pixels
- Signal readout via 9U NIM crate

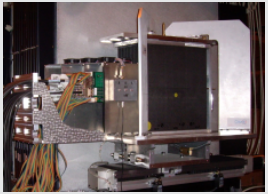

Technical Prototype

- Technical performance study.
- Developed since 2011.
- Large scale integration.
- Tests at low energies. (1–6 GeV)

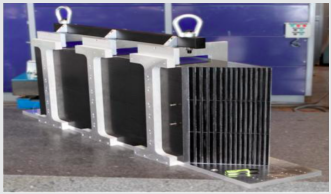

Technological Milestone

- Further technical challenges
- 15 layer assembly (1/2 ILD)
- Implement compact design.
- Tests at higher energies. (1–150 GeV)

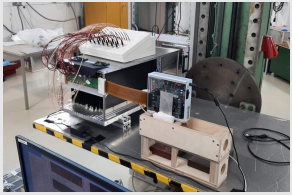

Beam Test at CERN

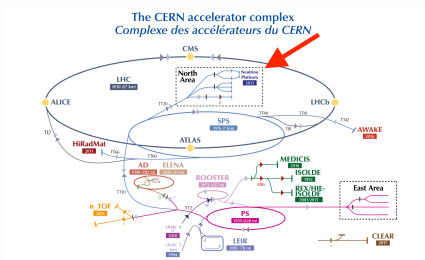

Particle Type	Energy [GeV]
Electron	10, 20, 40, 60, 80, 100, 150
Pion	10, 20, 70, 100, 150, 200
Muon	50, 150

Beam Test at CERN

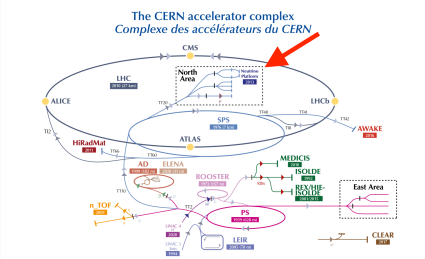

Particle Type	Energy [GeV]
Electron	10, 20, 40, 60, 80, 100, 150
Pion	10, 20, 70, 100, 150, 200
Muon	50, 150

Commissioning

Calibration constants

- Pedestal values
  - 15 layers / 16 chips / 64 channels / 15 SCAs
- $+1$ MIP scaling
- $\times$ 2 gains
- 491,520 parameters

Commissioning steps

1. Masking
2. Noise threshold determination
3. Pedestal calibration
4. MIP calibration
5. Trigger threshold determination
6. Hold scan

Commissioning

Calibration constants

- Pedestal values
  - 15 layers / 16 chips / 64 channels / 15 SCAs
- $+1$ MIP scaling
- $\times$ 2 gains
- 491,520 parameters

Commissioning steps

1. Masking
2. Noise threshold determination
3. Pedestal calibration
4. MIP calibration
5. Trigger threshold determination
6. Hold scan

Masking Results

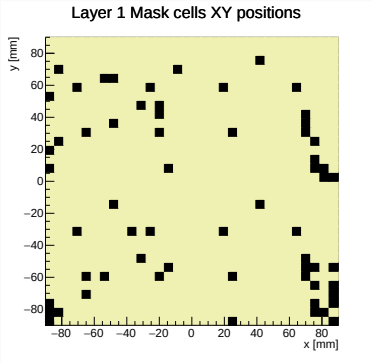

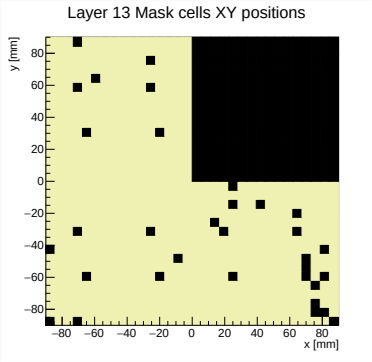

- Electrical cross talks.
- Connection to the readout board.

- Sensor delamination.
- Issues with conductive glue attachment.

MIP Calibration

- Muon with the order of GeV is a good approximation of MIP.
- Charge measurement after the pedestal subtraction.
- Gauss-Landau convolution function used to extract MIP value.

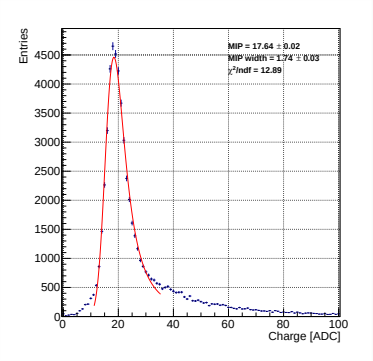

Figure 1: Mean MIP val. for layer 7, ASIC 6, high gain. Pedestal subtracted.

Analysis

Beam test simulation

- Simulation was conducted for the SiW-ECAL prototype with the identical environment as the beam test setup.
- `Geant4` toolkit was used with geometrical parameters provided by `DD4HEP` framework.
- Beam size and position determined from the data.
- Identical maskings applied.

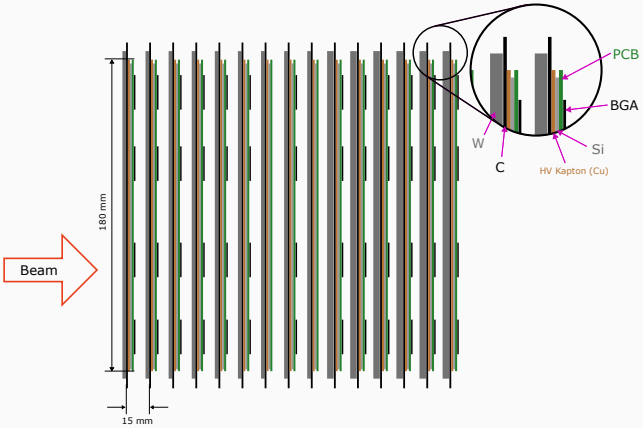

Beam test simulation

- Simulation was conducted for the SiW-ECAL prototype with the identical environment as the beam test setup.
- `Geant4` toolkit was used with geometrical parameters provided by `DD4HEP` framework.
- Beam size and position determined from the data.
- Identical maskings applied.

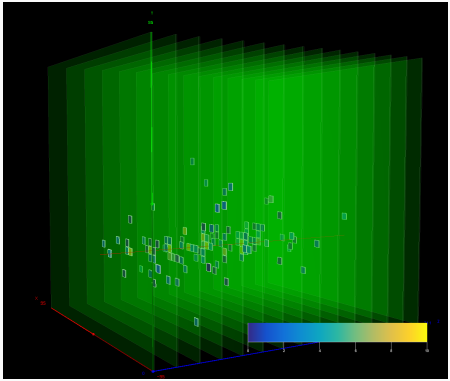

Event Building

- Event building was performed by merging the hits with the same time stamp.

Event Selection

- **Minimum energy**
  A hit is required to have minimum energy of 1 MIP.
- **Coincidence**
  Avoid the event reconstruction from the parasitic signals. Minimum of 13 layer coincidence is required.
- **Low Buffer Events**
  Beam hits occupy lower buffer range.
- **Hits in each layer**
  Further protection against parasitic signals:
  - Layer 0–7: At least one hit.
  - Layer 6–8: Minimum three hits.

Data & Simulation Comparison – Total Hits

Data/Simulation 10 GeV electron

Total hits

- Total number of hits for data and simulation are compared (normalized).
- Agreements in both data and simulation for the mean total number of hits.
- Discrepancy in lower and upper parts of distributions:
  - Parasitic hits.
  - Uncertainties in beam size and position for the simulation.

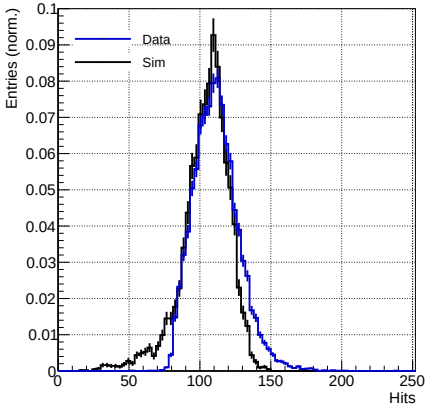

Data & Simulation Comparison – Hits per Layer

Data/Simulation 10 GeV electron

Hits per layer

- Number of hits registered in each layer.
- Shower maximum between layer 6–7.
- Dip in the distribution (particularly in layer 4) results from the delamination effect.
- Slight shift in shower peak between data/simulation.
- Possible cause:
  - Material content of the detector?
  - Start position of the beam in the simulation?

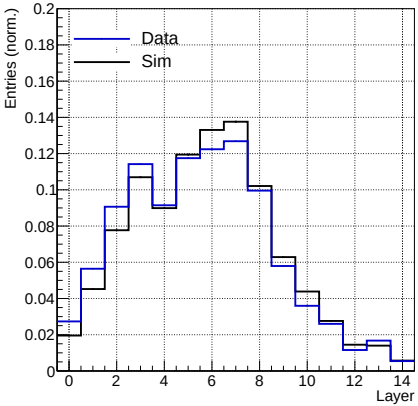

Data & Simulation Comparison – Total Energy

Total energy

- Fitted with a Gaussian curve and extracted energy mean and width.
- Peak energy around 580 MIPs.
- Observed energy resolution for simulation and reconstruction:

$$\frac{\sigma_{E_{sim}}}{E_{sim}} = 12.5 \pm 0.3\ (\text{stat.})\ \%$$
$$\frac{\sigma_{E_{reco}}}{E_{reco}} = 13.6 \pm 0.2\ (\text{stat.})\ \%$$

Without masking (simulation)

$$\frac{\sigma_{E_{sim}}}{E_{sim}} = 7.67 \pm 0.085\ (\text{stat.})\ \%$$

Data/Simulation 10 GeV electron

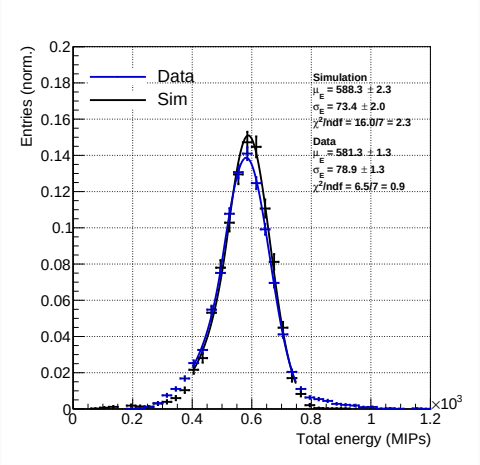

Conclusion for the Hardware Part

Conclusion

- Technical tests of the SiW-ECAL prototype were conducted, assembling 15 layers of FEVs.
- Beam test data of 10 GeV electron beam was processed.
- Excellent agreement between data and simulation for the EM shower energy resolution.
  - Data: **13.6%** $\pm$ **0.2%** (stat.)
  - Simulation: **12.5%** $\pm$ **0.3%** (stat.)
- Identified and understood the problems for the current SiW-ECAL prototype.

Outlook

- Reduce masking
  - Improper routing on the PCB.
- New iterations of the PCBs.
- Investigation on sensor delamination .
  - Initiated in both IFIC and IJCLab.

Light Quark Pair Production

Physics Beyond Standard Model

- Fermion mass hierarchy is not explained by the SM.
- BSM theories (i.e. Randal Sundrum, Gauge Higgs Unification...) predict resonance coupling to the heavy flavor doublet (t, b) and also to the light quarks (c, s, u, d).
- Measure Z' resonance coupling to fermion pair at per mil level.

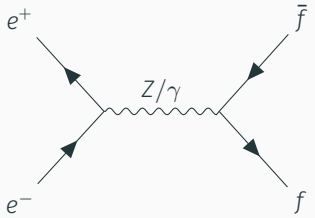

Differential Cross Section

For $e^+e^- \to V \to f\bar{f}$ process,

$$\frac{d\sigma_{LR}^{f\bar{f}}}{d\cos\theta} = \Sigma_{LL}(1+\cos\theta)^2 + \Sigma_{LR}(1-\cos\theta)^2$$
$$\frac{d\sigma_{RL}^{f\bar{f}}}{d\cos\theta} = \Sigma_{RR}(1+\cos\theta)^2 + \Sigma_{RL}(1-\cos\theta)^2$$

where Σ_{ij} are the helicity amplitudes as function of g_L, g_R. The variable θ is the scattering angle of a fermion.

Forward-Backward Asymmetry

$$A_{FB} \equiv \frac{\sigma(\cos\theta > 0) - \sigma(\cos\theta < 0)}{\sigma(\cos\theta > 0) + \sigma(\cos\theta < 0)}$$

Ratio of forward-backward cross section

→ Leads to cancellation of some systematic errors.

- The Z' coupling to a fermion pair give observables polar angle dependence.
- Beam polarization give access to all four helicity amplitudes.

Event Generation & Simulation

Generation

- Monte Carlo generators
  - `WHIZARD 2.8.5`
  - `PYTHIA 6.4`
- Hadronization tune: OPAL experiment.
- Generator setup:
  - $e^+e^- \to q\bar{q}$
  - $\sqrt{s} = 250\,\text{GeV}$
  - $(\mathcal{P}_{e^-}, \mathcal{P}_{e^+}) = (\mp 1.0, \pm 1.0)$
  - ISR
- SM background processes with multi-quark final state.
  - WW, ZZ, $q\bar{q}H$

Simulation

- Full detector simulation of ILD (`ILD_l5_o1` model)
  - `GEANT4`

Reconstruction

- Reconstruction tool
  - `ILCSoft v02-03-02`

Integrated Luminosity [fb^{-1}]

Process	$e_L^- e_R^+$	$e_R^- e_L^+$
$q\bar{q}$	4994	4994
$WW \to 4q$	4996	5116
$ZZ \to 4q$	5052	5109
$q\bar{q}H$	1457	2278

Signal $\sigma_{e^+e^- \to q\bar{q}}$ [fb]		
Process	$e_L^- e_R^+$	$e_R^- e_L^+$
$d\bar{d}$	4484.52	988.93
$u\bar{u}$	6548.26	2772.10
$s\bar{s}$	4442.36	979.51
$c\bar{c}$	6573.02	2782.64
$b\bar{b}$	4566.99	1007.46
Background $\sigma_{e^+e^- \to X}$ [fb]		
$WW \to 4q$	14867.8	136.8
$ZZ \to 4q$	1405.2	606.7
$q\bar{q}H$	343.0	219.5

Event Topology

Event Topology

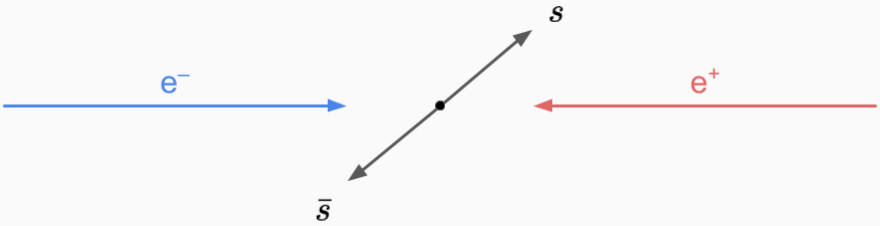

Event Topology

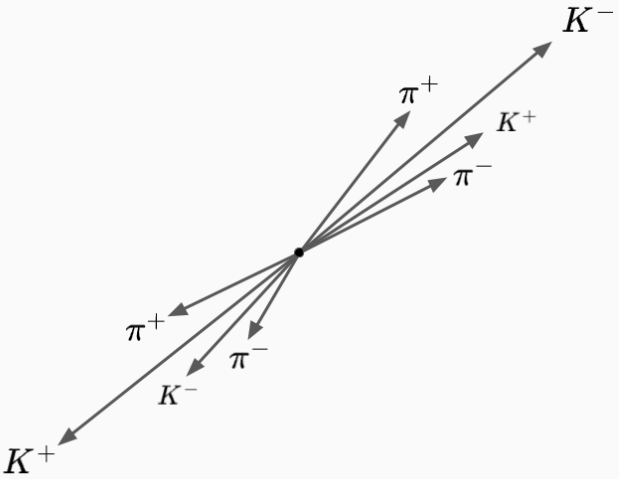

Event Topology

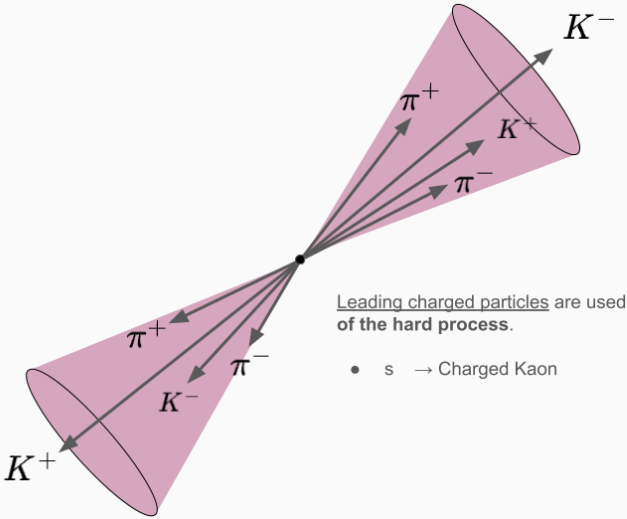

Leading charged particles are used as **imprint of the hard process**.

- s → Charged Kaon

Event Topology

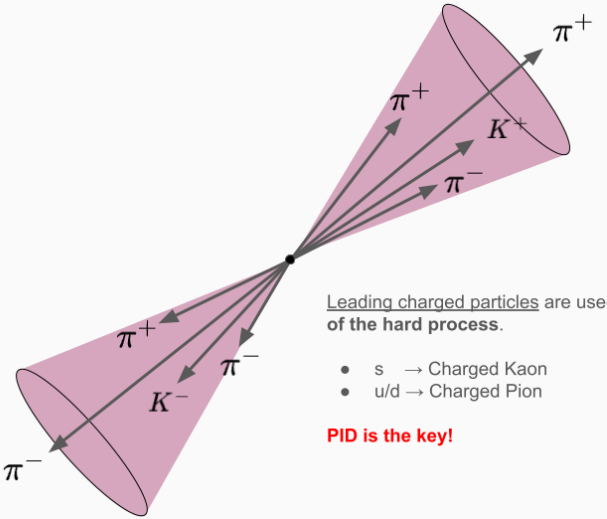

Leading charged particles are used as **imprint of the hard process**.

- s → Charged Kaon
- u/d → Charged Pion

PID is the key!

Event Topology

Di-jet system

- Jet acollinearity: $\sin\psi_{acol} < 0.9$
- Di-jet mass: $m_{j_1,j_2} > 140\ \mathrm{GeV}$
- Jet-distance: $y_{23} < 0.02$

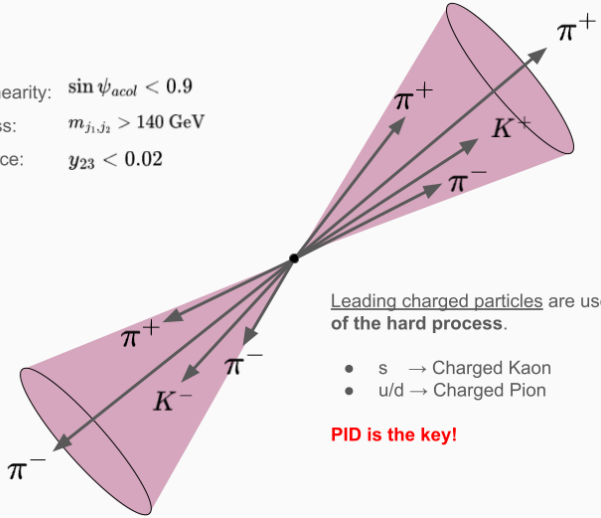

Leading charged particles are used as **imprint of the hard process**.

- s → Charged Kaon
- u/d → Charged Pion

PID is the key!

Preselection of Di-jet events

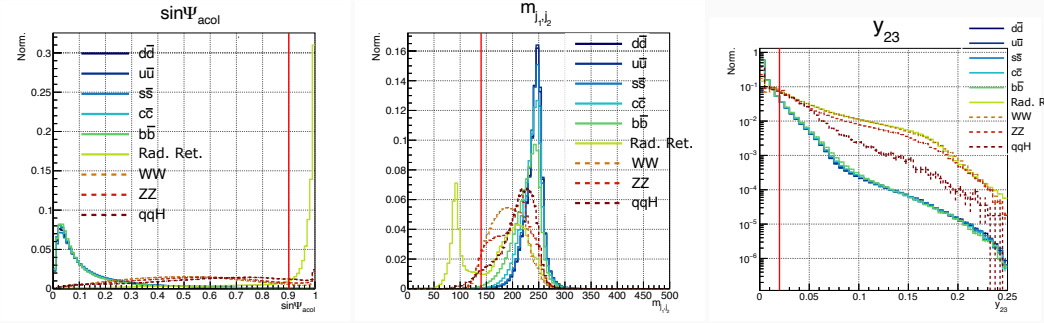

Figure 2: Three histograms illustrating the variable ($\sin\Psi_{acol}$, m_{j_1,j_2}, y_{23}), each successively refined by applying a cut on the left histogram. Red line shows the cut.

Light Quark Selection

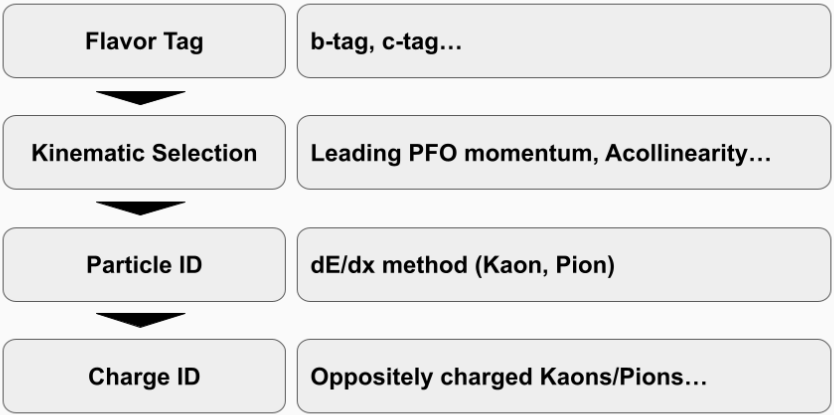

Light Quark Selection

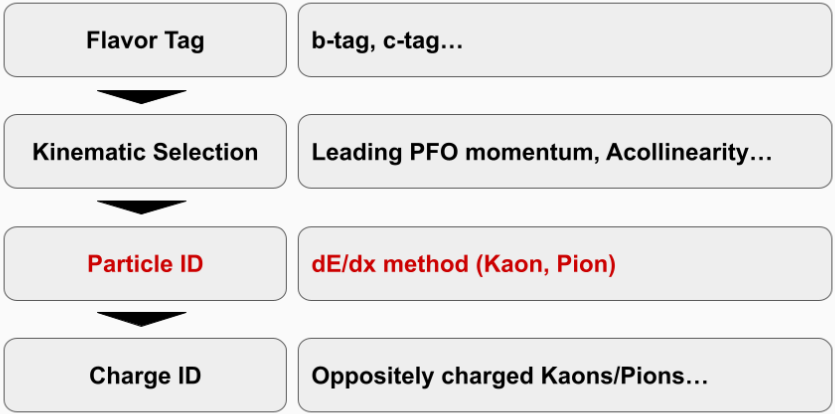

Bethe-Bloch formula

Mean energy loss of particle per distance

$$-\frac{dE}{dx} = Kz^2 \frac{Z}{A} \frac{1}{\beta} \left[\frac{1}{2} \ln f(\beta) - \beta^2 - \frac{\delta(\beta\gamma)}{2} \right]$$

- Bethe-Bloch formula tells each particle type as unique dE/dx vs p function.

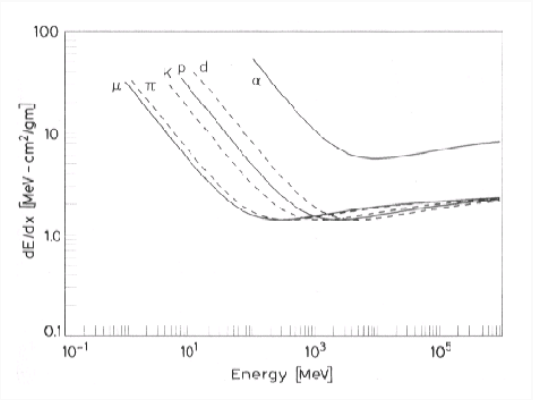

dE/dx Particle Identification

- TPC provides information on average dE/dx values for each track.
- Particle ID performed by choosing the phase-space region where it is dominated by the particle of interest.
- Main particles are $K^{\pm}$, $\pi^{\pm}$ and p ($\bar{p}$).
- Electron and muon contributions are negligible.

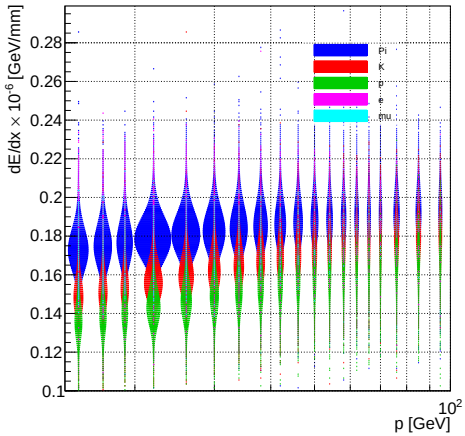

Figure 3: dE/dx vs p for light quark samples.

dE/dx distance

dE/dx distance is defined as following:

$$\Delta_{dE/dx-i} = \left(\frac{dE/dx_{exp} - dE/dx_{i,BB}}{\Delta dE/dx_{exp}} \right)$$

separation between experimental and theoretical Bethe curve.

Identification

Minimize the dE/dx distance as:

$$min(\Delta_{dE/dx-\pi}, \Delta_{dE/dx-K}, \Delta_{dE/dx-p}) = \Delta_{dE/dx-K}$$

dE/dx closest to the theoretical Kaon Bethe curve.

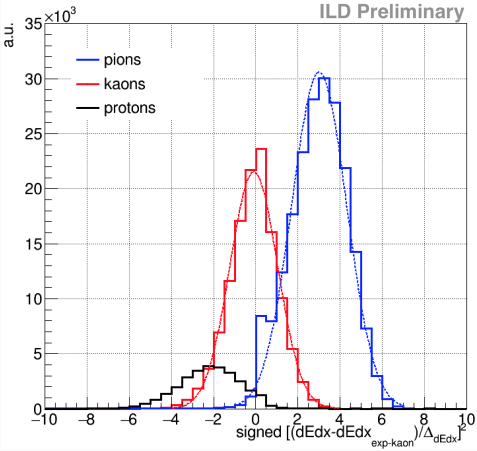

Figure 4: dE/dx distance for $s\bar{s}$ sample with PFO above $p > 15$ GeV.

dE/dx distance

dE/dx distance is defined as following:

$$\Delta_{dE/dx-i} = \left(\frac{dE/dx_{exp} - dE/dx_{i,BB}}{\Delta dE/dx_{exp}} \right)$$

separation between experimental and theoretical Bethe curve.

Identification

Minimize the dE/dx distance as:

$$min(\Delta_{dE/dx-\pi}, \Delta_{dE/dx-K}, \Delta_{dE/dx-p}) = \Delta_{dE/dx-K}$$

dE/dx closest to the theoretical Kaon Bethe curve.

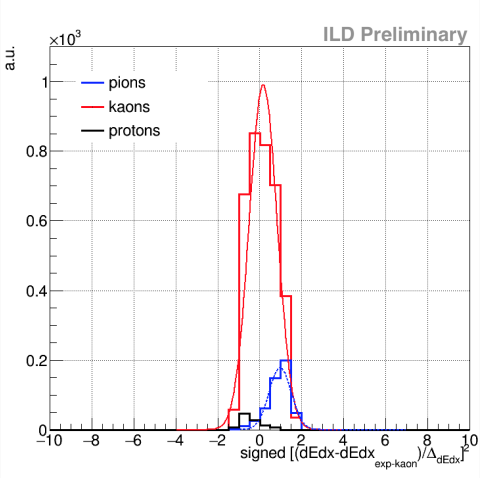

Figure 4: dE/dx distance for $s\bar{s}$ sample with PFO above $p > 15$ GeV.

Event Selection Efficiency

Cuts	Fraction of events after cut (Number of events)				
	$d\bar{d}$	$u\bar{u}$	$s\bar{s}$	$c\bar{c}$	$b\bar{b}$
None	100% (2.01e7)	100% (2.94e7)	100% (1.99e7)	100% (2.94e7)	100% (2.03e7)
Flavor tag + Kinematic	44.9%	49.1%	41.7%	3.48%	0.050%
Pion ID	13.7%	13.7%	5.92%	0.438%	0.007%
Final	1.75%	2.04%	0.889%	0.102%	0.003%

Table 1: Selection efficiency for the $e^+e^- \to u\bar{u}/d\bar{d}$ using Pions for $e_L^- e_R^+$ beam polarization.

Event Selection Efficiency

Cuts	Fraction of events after cut (Number of events)				
	$d\bar{d}$	$u\bar{u}$	$s\bar{s}$	$c\bar{c}$	$b\bar{b}$
None	100% (2.01e7)	100% (2.94e7)	100% (1.99e7)	100% (2.94e7)	100% (2.03e7)
Flavor tag + Kinematic	44.9%	49.1%	41.7%	3.48%	0.050%
Kaon ID	1.61%	1.94%	4.91%	0.276%	0.003%
Final	0.198%	0.296%	0.625%	0.056%	0.000%

Table 2: Selection efficiency for the $e^+e^- \to s\bar{s}$ using Kaons for $e_L^- e_R^+$ beam polarization.

Results

Kaon polar angle

- The K^- polar angle distribution.
- Pure $s\bar{s}$ sample for $e_L^- e_R^+$ polarization.
- Excellent agreement between the reconstructed and parton level polar angles.
- Drop in an efficiency at the forward region due to the detector acceptance.

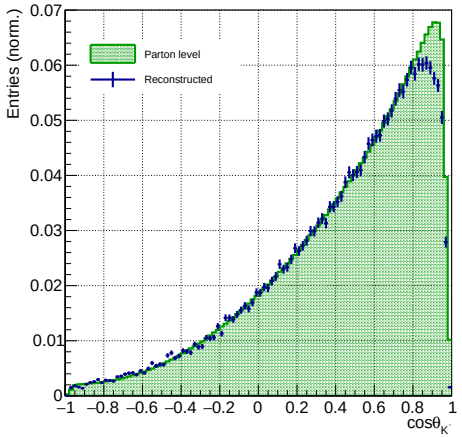

Polar Angle Distribution - $s\bar{s}$

Kaon polar angle

- The K^- polar angle distribution.
- Pure $s\bar{s}$ sample for $e^-_R e^+_L$ polarization.
- Excellent agreement between the reconstructed and parton level polar angles.
- Drop in an efficiency at the forward region due to the detector acceptance.

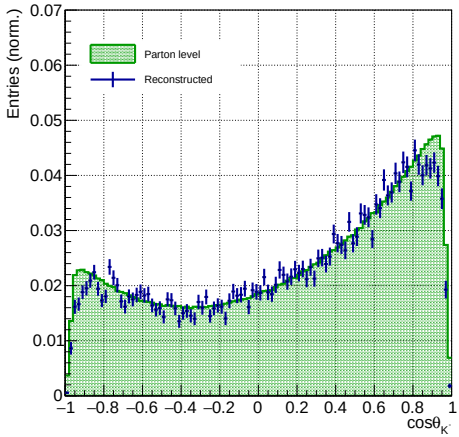

Signal and Background processes

- The K^- polar angle distribution for signal and background processes.
- $e_L^- e_R^+$ polarization sample.
- Scaled to each integrated luminosity.
- Primary backgrounds for the $s\bar{s}$ are the $u\bar{u}$ and $d\bar{d}$ processes.

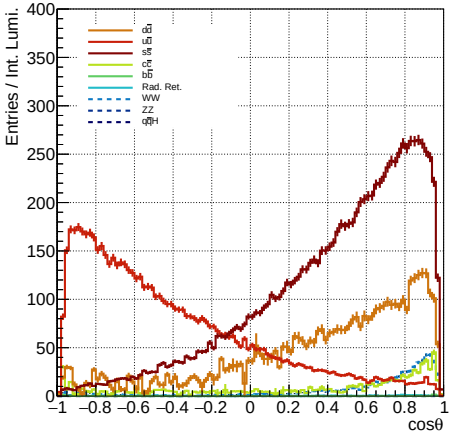

Polar Angle Distribution - $s\bar{s}$

Signal and Background processes

- The K^- polar angle distribution for signal and background processes.
- $e^-_R e^+_L$ polarization sample.
- Low number of entries due to low cross section for the right handed process.

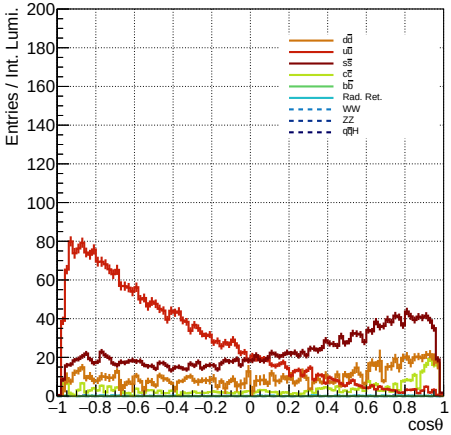

Background subtraction

- Background events were subtracted from the total distribution.
- $e_L^- e_R^+$ polarization sample.
- Conservative estimate on systematic uncertainty by assuming 5% uncertainty in background identification, reflected in the error bars.
- Polar angle fit with

$$\frac{d\sigma}{d\cos\theta} = S(1+\cos^2\theta) + A\cos\theta$$

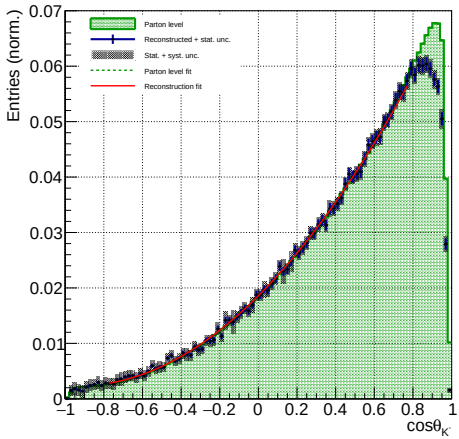

Background subtraction

- Background events were subtracted from the total distribution.
- $e_R^- e_L^+$ polarization sample.
- Consistency between reconstructed and parton level polar angles, along with their fits.

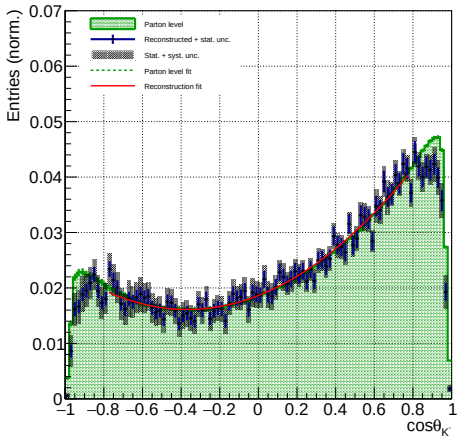

Polar angle fits

- Polar angle fit results for both polarizations.
- Method for the Kaon identification was focused to achieve higher purity.
- Results with small systematic uncertainty respect to the original *S* and *A* parameter predicted in the parton level.

		S	σ_S	A	σ_A
$e_L^- e_R^+$	Gen	1.86e-2	1.54e-5	3.51e-2	4.35e-5
	Reco	1.85e-2	1.06e-4	3.48e-2	2.89e-4
$e_R^- e_L^+$	Gen	1.86e-2	4.00e-5	1.35e-2	1.10e-4
	Reco	1.86e-2	2.20e-4	1.37e-2	6.16e-4

	$\sigma_{S_{sys.}}$	$\sigma_{A_{sys.}}$
$e_L^- e_R^+$	5.08e-5	8.68e-5
$e_R^- e_L^+$	1.24e-4	2.08e-4

Polar Angle Distribution - $u\bar{u}/d\bar{d}$

Signal and Background processes

- The π^- polar angle distribution for signal and background processes.
- $e_L^- e_R^+$ polarization sample.
- Backward region mainly dominated by the $u\bar{u}$ signals.

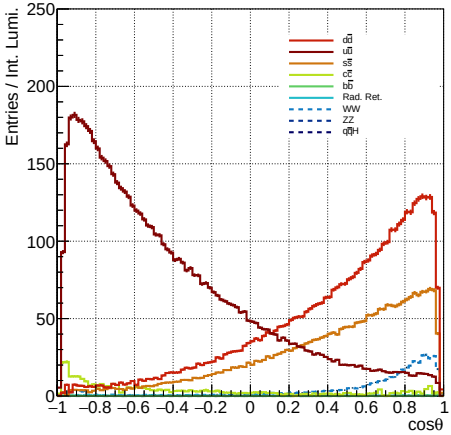

Polar Angle Distribution - $u\bar{u}/d\bar{d}$

Signal and Background processes

- The π^- polar angle distribution for signal and background processes.
- $e_R^- e_L^+$ polarization sample.
- Backward region mainly dominated by the $u\bar{u}$ signals.

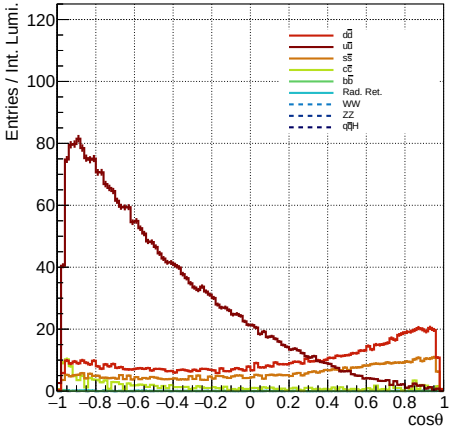

Polar Angle Distribution - $u\bar{u}/d\bar{d}$

Background subtraction

- Background events were subtracted from the total distribution.
- $e_L^- e_R^+$ polarization sample.
- Assuming 5% uncertainty in background identification.
- Agreement in the barrel region of the polar angle.

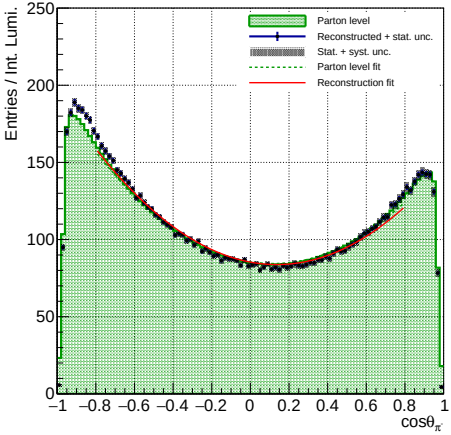

Polar Angle Distribution - $u\bar{u}/d\bar{d}$

Background subtraction

- Background events were subtracted from the total distribution.
- $e_R^- e_L^+$ polarization sample.
- Assuming 5% uncertainty in background identification.
- Agreement in the overall region of the polar angle.

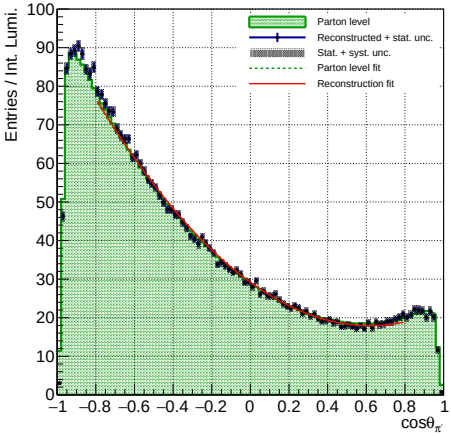

Polar angle fits

- The S and A are the fit parameters, which corresponds to the terms associated with $\cos^2\theta$ and $\cos\theta$.
- Fit region restricted to $|\cos\theta| < 0.8$ in order to capture the barrel region.
- $u\bar{u}$ distribution can benefit from the fact that it has large polar region where it is less contaminated by the backgrounds for both polarizations.

		S	σ_S	A	σ_A
$e_L^- e_R^+$	Gen	85.7	0.026	-20.2	0.073
	Reco	85.4	0.175	-23.4	0.495
$e_R^- e_L^+$	Gen	29.2	0.015	-35.5	0.040
	Reco	29.2	0.088	-36.2	0.246

	$\sigma_{S_{sys.}}$	$\sigma_{A_{sys.}}$
$e_L^- e_R^+$	0.110	0.306
$e_R^- e_L^+$	0.050	0.144

- Statistical uncertainty for the cross section of $e^+e^- \to s\bar{s}$ process is calculated.

$$\frac{\sigma_{stat}}{\sigma} = \sqrt{\left(\frac{\delta N}{N}\right)^2 + \left(\frac{\delta \mathcal{L}_{int}}{\mathcal{L}_{int}}\right)^2 + \left(\frac{\delta \mathcal{P}_e}{\mathcal{P}_e}\right)^2}$$

- Luminosity measurement at ILC can be achieved with uncertainty of 0.1%.
- Polarization uncertainty at ILC is estimated to be 0.25% for the full polarization.
- Final calculated cross section for $s\bar{s}$ was measured with statistical uncertainty of **0.340%** for $e_L^- e_R^+$ and **0.694%** for $e_R^- e_L^+$ polarization.

Forward-Backward Asymmetry value was calculated from the S and A parameters from the fits, along with its statistical and systematical uncertainties.

$$A_{FB} = \frac{3A}{8S}$$

uu and dd with Pion ID

Polarization	A_{FB}^{gen}	A_{FB}^{reco}	δA_{FB}^{stat}	δA_{FB}^{sys}
$e_L^- e_R^+$	-8.75e-2	-9.94e-2	1.18e-4	9.48e-3
$e_R^- e_L^+$	-4.56e-1	-4.64e-1	1.76e-4	1.45e-2

ss with Kaon ID

Polarization	A_{FB}^{gen}	A_{FB}^{reco}	δA_{FB}^{stat}	δA_{FB}^{sys}
$e_L^- e_R^+$	0.709	0.702	1.00e-4	1.67e-3
$e_R^- e_L^+$	0.272	0.275	2.85e-4	4.10e-3

Conclusion and Outlook for the Light Quark Analysis

Conclusion

- Light pair production process ($e^+e^- \to u\bar{u}, d\bar{d}, s\bar{s}$) for ILC $\sqrt{s}$ =250 GeV with ILD full detector simulation.
- dE/dx information from the TPC was used for the PID method.
- The final cross section measurement result for $s\bar{s}$ events has shown the precision of 0.340% for $e_L^- e_R^+$ and 0.694% for $e_R^- e_L^+$.
- Forward-backward asymmetry demonstrated the ILC's capability on its precision measurement for light quark pair production process.

Outlook

- Improvement in the dE/dx PID resolution.
- Recent development on cluster counting method revealed it can further improve the separation with dE/dx resolution up to 3.5%, leading to further purify the PID selection.
- Computation of Z' to fermion pair coupling with the extracted A_{FB}.

Talks and Reviewed Publications

Conference name	Place	Date
CALICE Collaboration Meeting	Orsay, FR	08/09/2021
Lepton Photon 2021	Manchester, UK	10/01/2022
CALICE Collaboration Meeting	Valencia, ES	22/04/2022
ICHEP 2022	Bologna, IT	08/07/2022
CALICE Collaboration Meeting	Palaiseau, FR	12/10/2022
CALICE Collaboration Meeting	Göttingen, DE	31/03/2023
The 2023 International Workshop on CEPC	Edingurg, UK	04/07/2023
Higgs Hunting 2023	Paris, FR	13/09/2023
CALICE Collaboration Meeting	Prague, CZ	28/09/2023
Second Workshop on e^+e^- Higgs/WE/Top Factories	Paestrum, IT	11/10/2023

Talks and Reviewed Publications

Publication title	Date	DOI
Strange Quark Pair Production in High Energy Electron Positron Collisions	30/06/2022	10.5281/zenodo.6784638
Quark production in high energy electron positron collisions: from strange to top	15/06/2023	10.22323/1.414.0871

Thank you!

Backup

SKIROC Schematic

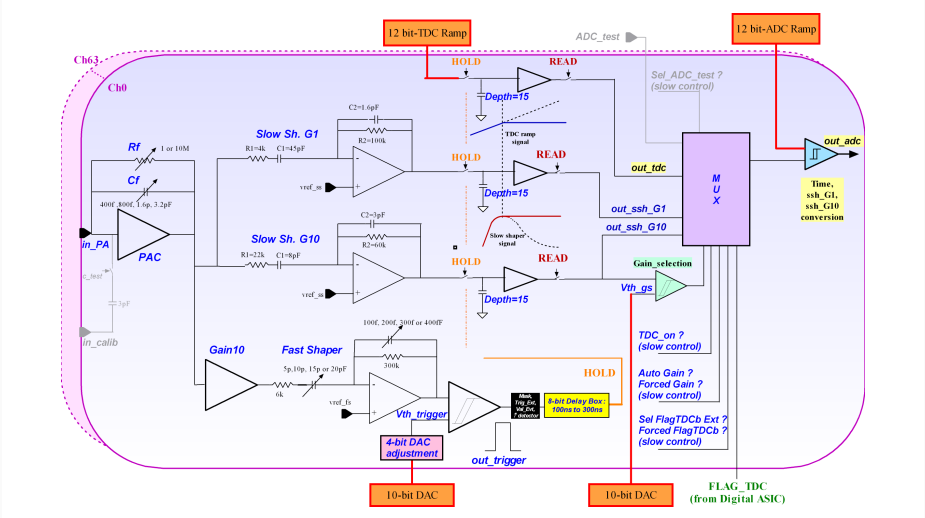

Front End Board

FEV 10–12

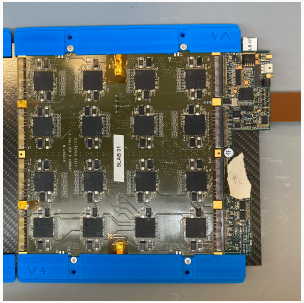

- ASICs in the BGA package.
- Main “working houses” since 2014.

COB

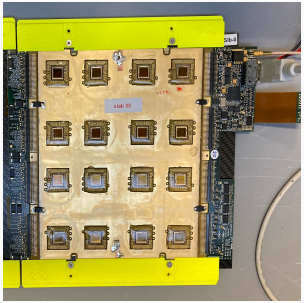

- Chip On Board (COB).
- ASICs wire bonded cavities.
- Thinner than FEV with BGA.

FEV 13

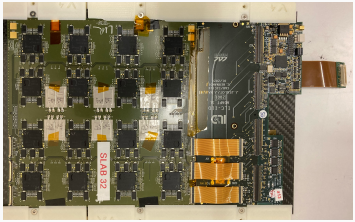

- ASICs based on BGA packaging.
- Different routing than FEV 10–12.
- Different external connectivity.

Noisy Cells

- There are 15,360 cells in overall SiW-ECAL.
- Some of which were required to be masked due to:
  - Electrical cross talk.
  - Sensor delamination.
  - Connector to the SL-Board.
- Required relatively high threshold for all cells in each step.
- Progressively lowered threshold, ranging from 350–275 DAC.

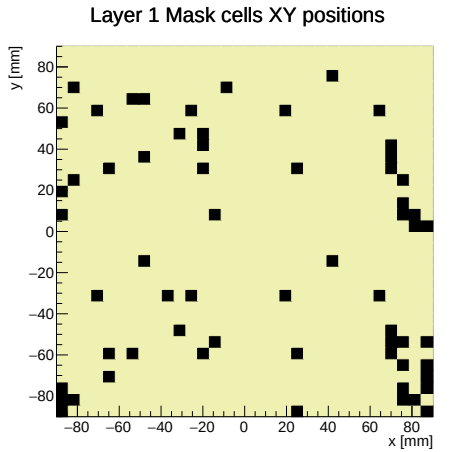

Cell Masking

Noisy Cells

- There are 15,360 cells in overall SiW-ECAL.
- Some of which were required to be masked due to:
  - Electrical cross talk.
  - Sensor delamination.
  - Connector to the SL-Board.
- Required relatively high threshold for all cells in each step.
- Progressively lowered threshold, ranging from 350–275 DAC.

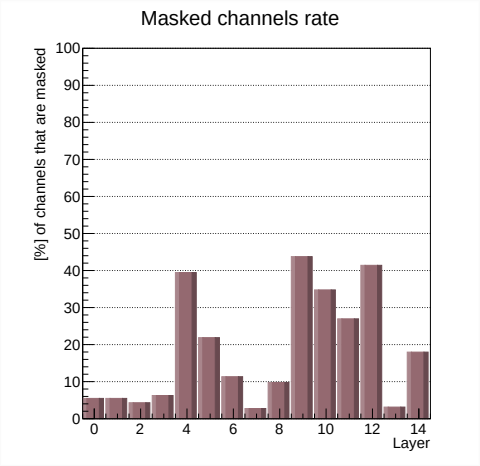

Noise Threshold Determination

Noise threshold

DAC threshold where the cell is not over saturated by the noise hits.

Procedure

- Number of hits were recorded for varying threshold values.
- Distribution was fitted with an error function.

$$f(x) = p_0 \cdot erfc\left(\frac{x - p_1}{p_2}\right)$$

$$erfc(z) = \frac{2}{\sqrt{\pi}} \int_z^\infty e^{-t^2} dt$$

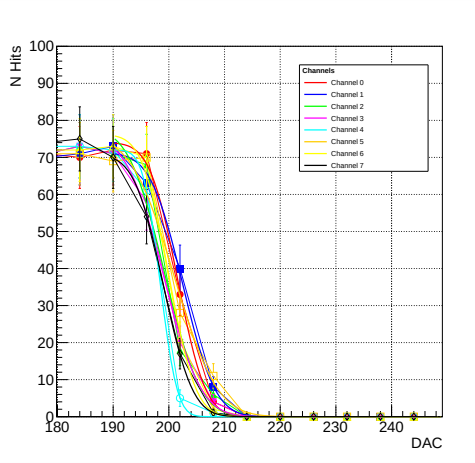

Pedestal Calibration

- Pedestal is the mean of the ADC values for all channels without any triggers.
- Total parameters: 15 layers / 16 chips / 64 channels / 15 SCAs

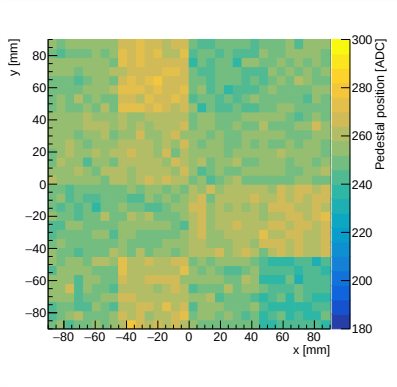

Figure 5: Fitted pedestal value for the first SCA of layer 7

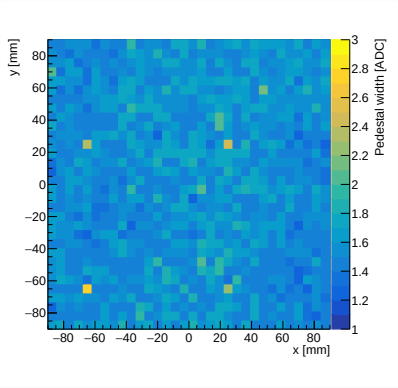

Figure 6: Width of the pedestal fit for the first SCA of layer 7

MIP Calibration

- 150 GeV muon beam was used to calibrate MIP values.
- Pedestal subtracted from the measured ADC values.

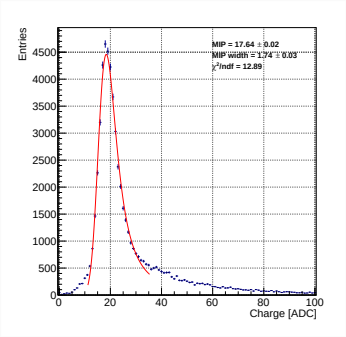

Figure 7: Mean MIP val. for layer 7, ASIC 6, high gain. Pedestal subtracted.

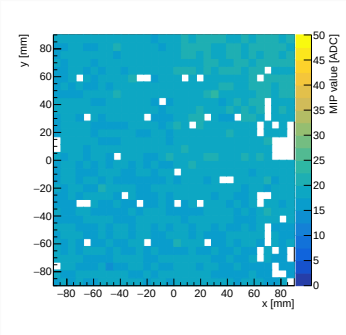

Figure 8: Mean MIP values in layer 7.

Trigger Threshold

- The objective is to measure signal >0.5 MIP.
- Using charge injection feature in SKIROC, 0.5, 0.75, 1.0 and 2.0 MIP pulse were injected.

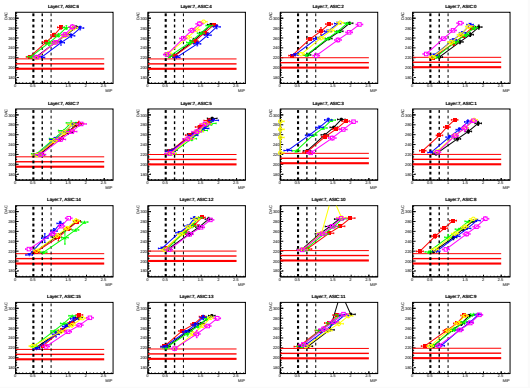

Figure 9: MIP injection in layer 7

Hold Scan

- Signal is needed to be read along the pulse that is generated by the slow shaper. This timing is managed by trigger delay.
  - Optimum trigger delay depends on the threshold.
- The delay-for-hold can be configured via DAQ software.
  - Inject the signal to row-by-row with signal amplitude of 1.2 V.
  - Hold sscan was performed from the range of 20–160 DAC in steps of 20.

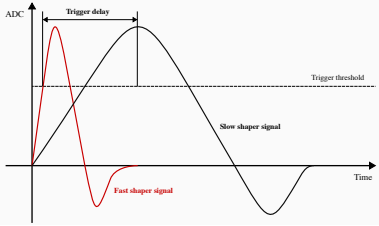

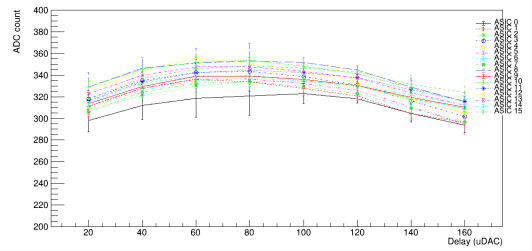

Sensor Delamination

Sensor delamination characteristics

- Mechanical detachment.
- Certain group of cells are constantly inactive.
- Issues with conductive glue detachment.

Possible cause

- Degradation of conductive adhesive.
  - In-homogeneous mixing of adhesives.
- Bending effect from the PCB.
  - Environmental effect. (e.g. temperature and humidity)
- Currently under investigation.
  - Initiated at IFIC and IJCLab.
  - Outside the scope of this thesis dissertation.

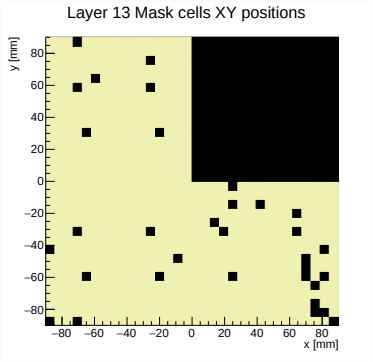

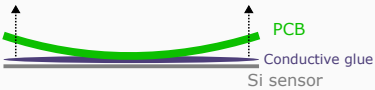

Power Pulsing

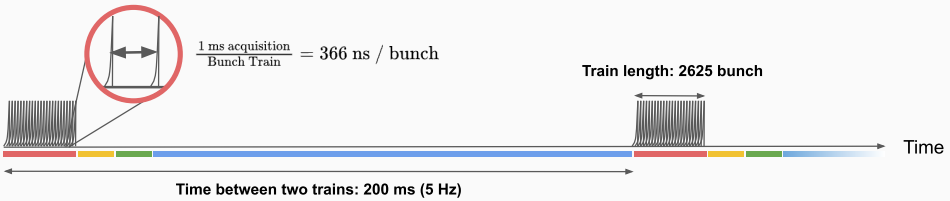

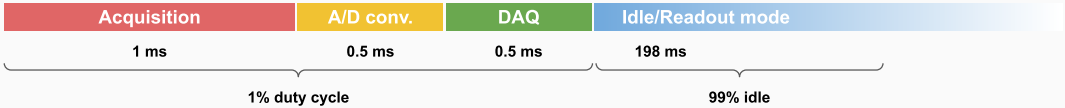

Hit Map

Hit distribution

- Hit position and ADC counts were recorded.
- 2D hit map shows the exact location where beam is hit.
- Beam position needs to be inputted for the simulation.
- First three layers were used to estimate the beam spot.

Extracted beam position

$$(x, y) = (-53.43\,\text{mm}, -41.73\,\text{mm})$$
$$(\sigma_x, \sigma_y) = (23.5\,\text{mm}, 29.7\,\text{mm})$$

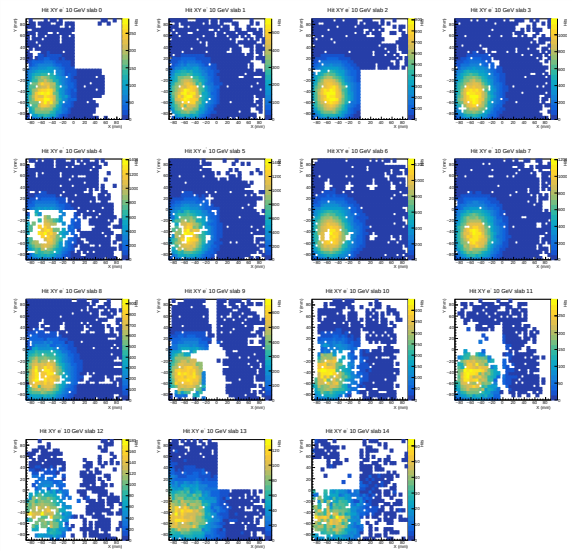

Hit Map

Hit distribution

- Hit position and ADC counts were recorded.
- 2D hit map shows the exact location where beam is hit.
- Beam position needs to be inputted for the simulation.
- First three layers were used to estimate the beam spot.

Extracted beam position

$$(x, y) = (-53.43\,\text{mm}, -41.73\,\text{mm})$$

$$(\sigma_x, \sigma_y) = (23.5\,\text{mm}, 29.7\,\text{mm})$$

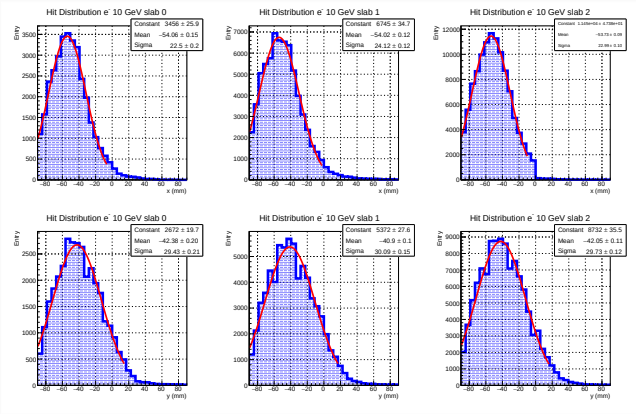

Hit Map

Simulated 10 GeV electron

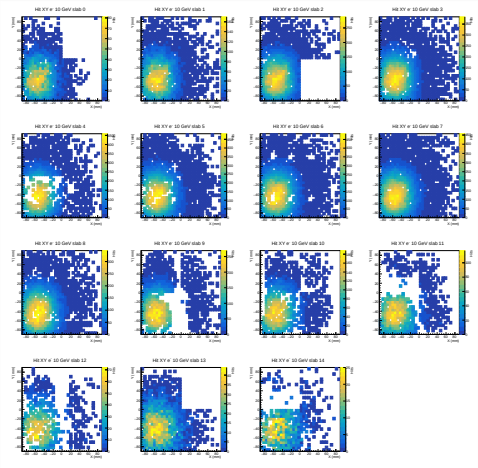

Data 10 GeV electron

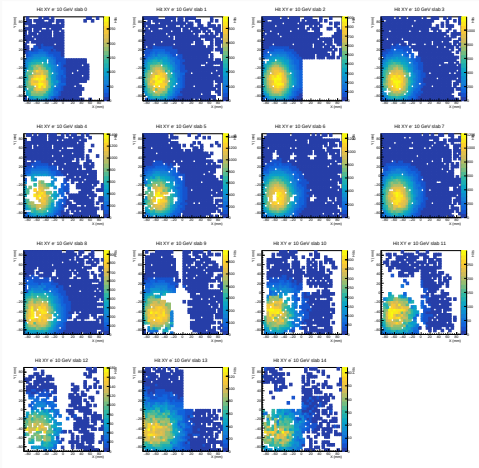

Towards ideal detector

- ILD ECAL proposes the energy resolution of order of $15\,\%/\sqrt{E}$.
- For 10 GeV electron, this is $\sigma E/E = 4.74\,\%$.
- The discrepancy originates from the difference in the sampling fraction between ILD and the SiW-ECAL prototype.

Sampling fraction

- **Number of layers**
  Full ILD setup with have 30 ECAL layers while the prototype has 15 layer.
- **Masking**
  Maskings were applied to the prototype, which further reduces the sampling fraction.

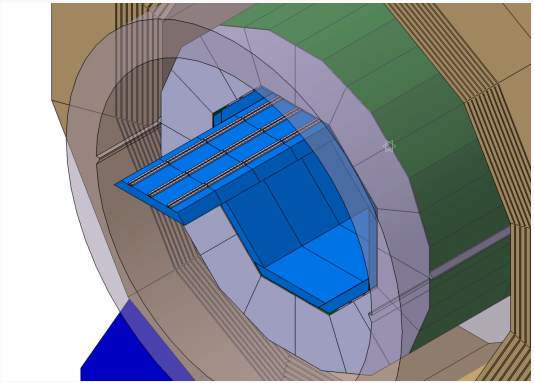

Total Energy Without Masking

Maskless simulation

- One can verify whether the final energy resolution can reach closer to the TDR proposed value without masking.
- Masking information was lifted for the simulation.
- Final energy resolution:

$$\frac{\sigma_{E_{sim}}}{E_{sim}} = 7.67 \pm 0.085 \text{ (stat.) } \%$$

Simulation 10 GeV electron

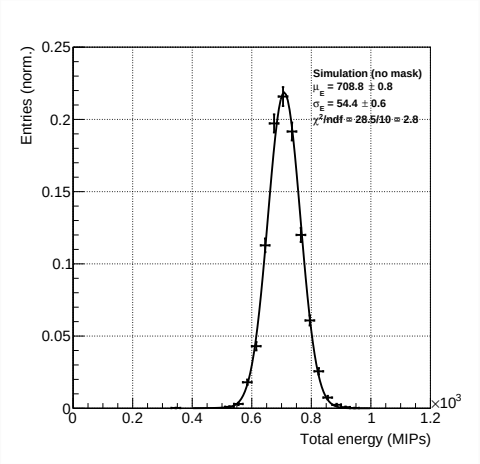

Event Reconstruction

- Jet/vertex reconstruction
- Flavor tagging

Background Rejection

- Photon veto
  - $E_\gamma < 115\,\mathrm{GeV}$
  - $|\cos\theta_\gamma| < 0.97$
- Acolinearity
  - $\sin\Psi_{acol} < 0.3$
- Invariant mass
  - $M_{j_1,j_2} > 140\,\mathrm{GeV}$
- Jet y_{23}
  - $y_{23} < 0.02$

Signal Definition

- Acolinearity of $q\bar{q}$
  - $\sin\Psi_{acol,q} < 0.9$
- Invariant mass
  - $M_{q\bar{q}} > 140\,\mathrm{GeV}$

Backgrounds

- Radiative return
- $e^+e^- \to WW \to 4f$
- $e^+e^- \to ZZ \to 4f$
- $e^+e^- \to q\bar{q}H$

Preselection of Di-jet events

	Signal					Background			
Process	dd	uu	ss	cc	bb	Rad. Ret.	WW	ZZ	qqH
$e_L^- e_R^+$	69.0%	69.8%	68.2%	69.7%	69.5%	0.5%	7.4%	7.5%	8.7%
$e_R^- e_L^+$	68.9%	69.8%	68.1%	69.8%	69.4%	0.5%	3.3%	8.1%	8.8%

Table 3: Percentage of remaining events after the entire background removal with left and right-handed electron beam polarization.

- All backgrounds including radiative return can be reduced down to few percent level.
- Signal processes all remain constantly around 60 % of the entire events.

Event Selection Efficiency

Cuts	Fraction of events after cut (Number of events)				
	$d\bar{d}$	$u\bar{u}$	$s\bar{s}$	$c\bar{c}$	$b\bar{b}$
None	100% (4.43e6)	100% (1.25e7)	100% (4.39e6)	100% (1.25e7)	100% (4.47e6)
Cut 1	94%	94.1%	93.3%	69.4%	1.06%
+ Cut 2	91.8%	91.8%	90.9%	12.3%	0.497%
+ Cut 3	89.7%	89.7%	88.8%	11.4%	0.427%
+ Cut 4	51.2%	56.2%	48.4%	4.17%	0.070%
+ Cut 5	46.4%	50.9%	43.9%	3.76%	0.060%
+ Cut 6	44.8%	49.1%	41.7%	3.48%	0.051%
+ Cut 7a	13.7%	13.7%	5.95%	0.440%	0.007%
+ Cut 8	1.75%	2.05%	0.896%	0.102%	0.003%

Table 4: Selection efficiency for the $e^+e^- \to u\bar{u}/d\bar{d}$ using Pions for $e_R^- e_L^+$ beam polarization.

Event Selection Efficiency

Cuts	Fraction of events after cut (Number of events)				
	$d\bar{d}$	$u\bar{u}$	$s\bar{s}$	$c\bar{c}$	$b\bar{b}$
None	100% (4.43e6)	100% (1.25e7)	100% (4.39e6)	100% (1.25e7)	100% (4.47e6)
Cut 1-6	44.8%	49.1%	41.7%	3.48%	0.051%
+ Cut 7b	1.59%	1.93%	4.89%	0.275%	0.003%
+ Cut 8	0.192%	0.293%	0.635%	0.055%	0.001%

Table 4: Selection efficiency for the $e^+e^- \to s\bar{s}$ using Kaons for $e^-_R e^+_L$ beam polarization.

Charge flip

- Migration occurs when reconstructing a particle charge opposite to its true charge in the parton level.
  - Mis-reconstruction from dE/dx distance PID.
  - Acceptance.
- Such mistake flips the reconstructed quark angle.

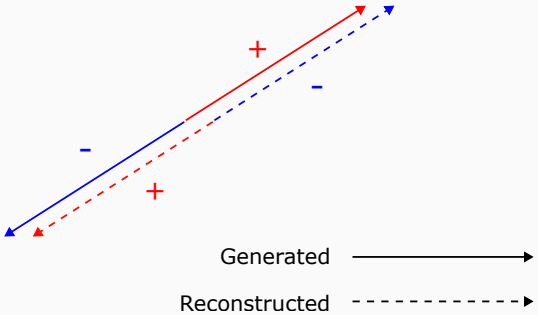

Light Quark Selection

#	Name	Quantity	Description
1	b-tag	$btag < 0.3$	Reject events with b-like jets
2	c-tag	$ctag < 0.65$	Reject events with c-like jets
3	nvtx	$nvtx = 1$	Jets should have only PV as vertex
4	Leading momentum	$p_{LPFO} > 15\,\text{GeV}$	Leading momentum cut
5	LPFO acollinearity	$\cos\theta_{LPFO_{1,2}} > 0.97$	LPFOs should be back-to-back
6	Offset	$V_0 = \sqrt{d_0^2 + z_0^2} < 1\,\text{mm}$	Offset cut to reject Λ_0 contribution
7a	dE/dx PID (π)	$dE/dx > 0.178 \times 10^{-6}\,\text{GeV mm}^{-1}$	$\pi^{\pm}$ identification
7b	dE/dx PID (K)	$min(\Delta_{dE/dx-(K,\pi,p)})$ for $\Delta_{dE/dx-K}$	$K^{\pm}$ identification
8	SPFO	Veto $p_{SPFO} > 10\,\text{GeV}$ and charge opposite to LPFO.	Attenuate the charge migration by rejecting oppositely charge LPFO competitor
9	Charge	$Q_{LPFO1} \times Q_{LPFO2} < 0$	Charge of LPFOs from both sides has opposite charge.

Light Quark Selection

#	Name	Quantity	Description
1	b-tag	$btag < 0.3$	Reject events with b-like jets
2	c-tag	$ctag < 0.65$	Reject events with c-like jets
3	nvtx	$nvtx = 1$	Jets should have only PV as vertex
4	Leading momentum	$p_{LPFO} > 15\,\text{GeV}$	Leading momentum cut
5	LPFO acollinearity	$\cos\theta_{LPFO_{1,2}} > 0.97$	LPFOs should be back-to-back
6	Offset	$V_0 = \sqrt{d_0^2 + z_0^2} < 1\,\text{mm}$	Offset cut to reject Λ_0 contribution
7a	dE/dx PID (π)	$dE/dx > 0.178 \times 10^{-6}\,\text{GeV mm}^{-1}$	$\pi^{\pm}$ identification
7b	dE/dx PID (K)	$min(\Delta_{dE/dx-(K,\pi,p)})$ for $\Delta_{dE/dx-K}$	$K^{\pm}$ identification
8	SPFO	Veto $p_{SPFO} > 10\,\text{GeV}$ and charge opposite to LPFO.	Attenuate the charge migration by rejecting oppositely charge LPFO competitor
9	Charge	$Q_{LPFO1} \times Q_{LPFO2} < 0$	Charge of LPFOs from both sides has opposite charge.

Separation power

Quantity to measure PID performance.

$$\eta_{A,B}(p) = \frac{|\mu_A - \mu_B|}{\sqrt{\frac{1}{2}(\sigma_A^2 - \sigma_B^2)}}$$

- Crossing of three dE/dx values near 1 GeV.
- Relativistic effect above 10 GeV.

Main competitor of Pion is Kaon.
Kaon suffers from both Pion and proton contamination...

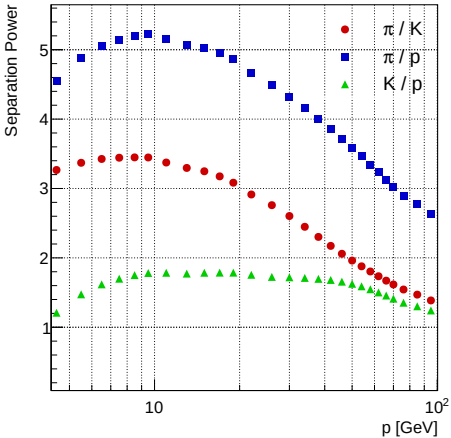

Pion ID & Kaon ID performance

- Selection purity and efficiency after cut 1-7.
- High Pion ID performance due to the background free region in the upper dE/dx.
- Kaon suffers suffers from the contamination from both Pion and Protons.

	Truth PID			
Reco. PID	$\pi^{\pm}$	$K^{\pm}$	$p\ (\bar{p})$	$e^{\pm}, \mu^{\pm}$
$\pi^{\pm}$	0.968	0.031	0.000	0.001
$K^{\pm}$	0.363	0.574	0.062	0.001
$p\ (\bar{p})$	0.015	0.363	0.579	0.043
Efficiency	0.968	0.575	0.605	-

Event Selection Efficiency

Cuts	Fraction of events after cut (Number of events)				
	$d\bar{d}$	$u\bar{u}$	$s\bar{s}$	$c\bar{c}$	$b\bar{b}$
None	100% (2.01e7)	100% (2.94e7)	100% (1.99e7)	100% (2.94e7)	100% (2.03e7)
Cut 1	94.1%	94.1%	93.2%	69.4%	1.06%
+ Cut 2	91.8%	91.8%	90.9%	12.3%	0.494%
+ Cut 3	89.7%	89.7%	88.8%	11.4%	0.423%
+ Cut 4	51.2%	56.1%	48.4%	4.17%	0.069%
+ Cut 5	46.5%	50.8%	43.9%	3.76%	0.058%
+ Cut 6	44.9%	49.1%	41.7%	3.48%	0.050%
+ Cut 7a	13.7%	13.7%	5.92%	0.438%	0.007%
+ Cut 8	1.75%	2.04%	0.889%	0.102%	0.003%

Table 5: Selection efficiency for the $e^+e^- \to u\bar{u}/d\bar{d}$ using Pions for $e_L^- e_R^+$ beam polarization.

Event Selection Efficiency

Cuts	Fraction of events after cut (Number of events)				
	$d\bar{d}$	$u\bar{u}$	$s\bar{s}$	$c\bar{c}$	$b\bar{b}$
None	100% (2.01e7)	100% (2.94e7)	100% (1.99e7)	100% (2.94e7)	100% (2.03e7)
Cut 1-6	44.9%	49.1%	41.7%	3.48%	0.050%
+ Cut 7b	1.61%	1.94%	4.91%	0.276%	0.003%
+ Cut 8	0.198%	0.296%	0.625%	0.056%	0.000%

Table 5: Selection efficiency for the $e^+e^- \to s\bar{s}$ using Kaons for $e_L^- e_R^+$ beam polarization.